Terrain Following using Wide Field Optic Flow

Evan Slatyer⋆ and Robert Mahony⋆ and Peter Corke†
⋆ Department of Engineering, Australian National University,
ACT, 0200, AUSTRALIA, {firstname}.{lastname}@anu.edu.au
† School of Engineering Systems, Queensland University of Technology,
Brisbane, QLD, 4000, AUSTRALIA peter.corke@qut.edu.au

Abstract

Wall and terrain following is a challenging problem for small, fast, and fragile robot vehicles. This paper presents a robust algorithm based on wide field integration of optic flow. Solutions for two dimensional and three dimensional wall following is provided for vehicles with non-holonomic velocity constraints that ensure that the focus of expansion of the flow field is known. The potential of the proposed algorithm is demonstrated in a simulation environment.

1 Introduction

This paper is motivated by the need to increase the autonomy of small-scale dynamic robotic vehicles such as aerial rotorcraft and UAV fixed-wing drones. Such vehicles are often required to transit between tasks by tracking the unknown local terrain while avoiding obstacles.

For a small and fast mobile robot, following walls or terrain at relatively close distances is a challenging problem. Conventional sensors are too heavy (eg. laser scanners that can cope with outdoor conditions), unsuitable for high-speed fragile robots (eg. tactile sensors), or too slow and inaccurate for the task considered (eg. ultrasound, IR sensors, etc). Vision sensors provide a low-cost, low-power, robust sensing paradigm suitable for navigation of small agile robotic vehicles in unstructured outdoor environments. Classical visual SLAM algorithms [Andreasson *et al.*, 2007; Davison *et al.*, 2007] are unsuitable for the wall tracking problem considered, since the distinctive feature points normally needed to build a SLAM map may not exist in an image sequence taken by a vehicle moving quickly and in close proximity to the surrounding environment. Even if such a features are available, any given feature is only visible for a few frames, and the cross correlation between features becomes a major limitation for the SLAM reconstruction [Kim and Sukkarieh, 2007; Bryson and Sukkarieh, 2007]. Other approaches make extensive assumptions about the nature of their environment [Vassallo *et al.*, 1998], limiting their flexibility. These difficulties can be overcome by working with optic flow and developing local reactive control strategies [Srinivasan *et al.*, 1999a; Muratet *et al.*, 2004], an approach strongly motivated by the study of behaviour of biological systems [Ruffier *et al.*, 2003]. Using optic flow for reactive control of robotic vehicles is a well established approach. Santos-Victor *et al.* demonstrated corridor centring and short-term wall following for a 2D wheeled robot using optic flow in 1995 [Santos-Victor *et al.*, 1995]. Coombs [Coombs *et al.*, 1995] utilised looming cues in the optic flow for obstacle avoidance and differential flow for corridor centring. Corridor centring control for a 2D hovercraft, without non-holonomic motion constraints, was done by Serres [Serres *et al.*, 2006]. More recently, corridor centring for a helicopter was demonstrated by Humbert *et al.* [Humbert *et al.*, 2009]. Terrain tracking, single wall following has also been extensively studied. Key work in this area is the biologically inspired methods investigated in the late nineties [Srinivasan *et al.*, 1996; 1999b], and more recent work [Zufferey and Floreano, 2005; 2006]. We also mention the recent work on terrain tracking by Herisse *et al.* [Herisse *et al.*, 2010].

In this paper, we propose a novel method for following walls or terrain using wide field optic flow. The proposed algorithm compares the measured optic flow field to a desired flow field pattern derived from an idealized model of an infinite planar wall. The key contribution of this paper is to show the derivative of the cost function defined in this manner can be computed from measured data. This is a non-trivial result since the optic flow depends on the unmeasured velocity of the vehicle as well as the unknown distance and orientation to the wall. The derivative of the cost function is used as a control input to the vehicle in a natural manner and the stability of the wall following behaviour is analysed using Lyapunov stability theory. The proposed algorithm is naturally resistant to noise in the optic flow field, and requires no

prior knowledge about the location or orientation of the wall or terrain to be tracked. It is highly robust to model error in the planar wall assumption since it averages over all observed flow and will stabilise to the dominant wall-like feature in the environment even if this feature is not flat. Moreover, the desired flow field pattern can be chosen to correspond to motion non-parallel to the wall. Thus, by choosing different target flow patterns the control can be used to regulate the vehicle to move away from the wall (obstacle avoidance) or towards the wall (docking), or steer parallel to the wall, in a single control framework.

In Section 2, the proposed algorithm is derived in two dimensions for a unicycle model with non-holonomic constraints on its velocity. Stability even when dense flow is unavailable is shown in Section 3. Simulation results for the 2D case are provided in Section 4, including a brief analysis of the effects of noise in the optic flow data. Section 5 generalises the algorithm to cover 3D vehicles with non-holonomic velocity constraints. Finally, Section 6 draws conclusions and suggests future directions for this work.

2 Non-holonomic vehicle moving in the plane.

In this section, the case of a ground-based, wheeled vehicle that can measure optic flow in a planar horizontal circle is considered. We assume that the environment consists of a single infinite wall and that the rotational optic flow is compensated using onboard gyrometer measurements or post-processing of the optic flow measurements [McCarthy *et al.*, 2008; Lim and Barnes, 2010]. The scenario is illustrated in Figure 1.

The optic flow for a two dimensional planar robot is modelled as a vector flow on the circle. Since the circle is orientable we use a scalar representation of the flow field where the flow is measured as positive in the anti-clockwise direction and vice-versa. The optic flow for a true robot consists of a term due to the translational velocity of the robot that also depends inversely on the range to local environment, and a second term that depends only on the angular velocity. When measurements of the angular velocity of the vehicle are available, such as those provided by gyrometers in a typical IMU, the angular velocity term can be directly compensated, and the remaining translational optic flow used for control [Zufferey and Floreano, 2005].

Based on the single planar wall assumption the scalar representation of translational flow is modelled by

$$\phi(\alpha;\theta,\mu) = \begin{cases} \mu \sin\alpha \sin(\alpha+\theta) & \text{for } -\theta < \alpha < \pi - \theta \\ 0 & \text{otherwise} \end{cases}$$

where $\mu = \frac{v}{d}$ is the scaled speed of the vehicle and θ is the orientation of the vehicle's body-fixed frame with respect

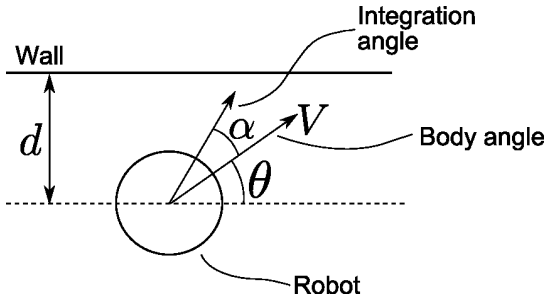

Figure 1: 2D non-holonomic scenario

to the world frame. Although the flow ϕ is measured, the variables d, v, and θ are not measured. Rather than working directly with ϕ we introduce an extended and normalised flow field λ on the full circle. Define

$$\kappa(\alpha;\theta,\mu) := \phi(\alpha;\theta,\mu) + \phi(\alpha+\pi;\theta,\mu). \tag{1}$$

The extended flow field κ is then normalised to compensate for the dependence on the unknown scaled velocity μ. Calculate the value of μ as

$$\mu = \sqrt{\frac{1}{\pi}\int_0^{2\pi} \csc^2\alpha\, \kappa^2(\alpha;\theta,\mu)\ \mathrm{d}\alpha} \tag{2}$$

and then define

$$\lambda(\alpha;\theta) := \frac{1}{\mu}\kappa(\alpha;\theta,\mu). \tag{3}$$

It is straightforward to verify that, for the scenario with a single infinite wall, the new flow variable λ has flow field

$$\lambda(\alpha;\theta) = \sin\alpha \sin(\alpha+\theta) \tag{4}$$

defined on the full circle. There are several advantages of working with the modified flow field λ. Firstly, since it is defined on the full circle, it simplifies the $\pi/2$ resampling process that we will use to compute the derivative of the flow field discussed below. Secondly, since the flow field from antipodal points is summed, the proposed flow field is zero when the vehicle is located in the centre of a corridor or room. As a consequence, control schemes based on λ will be true wall following schemes that allow free motion of the vehicle when there is no local wall or terrain to dominate the scene. This is an significant difference in the proposed approach to many of the existing approaches to wall and/or terrain following [Zufferey and Floreano, 2005; Serres *et al.*, 2006; Ruffier and Franceschini, 2005; Herisse *et al.*, 2010; Humbert *et al.*, 2009; Srinivasan *et al.*, 1999b]. Finally, note that although λ is normalised, the relative sensitivity to the environment retains the inverse $1/d$ range dependence characteristics of optic flow. Thus, the optical cue λ will be dominated by the local flow field and

distant parts of the environment will tend to be ignored leading the proposed wall/terrain tracking algorithm to follow the closest wall-like feature in the environment.

Let θ_r denote the desired angle that the robot tracks with respect to the wall. That is, setting $\theta_r = 0$ corresponds to tracking parallel to the wall. Choosing $\theta_r \in (0, \pi)$ specifies that the robot will approach the wall and would be used in a docking type manoeuvre. Setting $\theta_r \in (\pi, 2\pi)$ specifies that the robot diverges from the wall and would be used in applications such as obstacle avoidance. The goal of the control design is to adjust angular velocity of the robot to steer the orientation θ towards the desired orientation θ_r under the assumption that the speed of the vehicle is non-zero. This is achieved by steering $\lambda(\alpha, \theta)$ to $\lambda(\alpha, \theta_r)$.

In order to achieve this goal it is necessary to understand how λ varies with θ. Then

$$\begin{aligned}\frac{\partial}{\partial\theta}\lambda(\alpha;\theta) &= \sin\alpha\cos(\alpha+\theta)\\ &= \lambda(\alpha+\frac{\pi}{2};\theta)\tan\alpha.\end{aligned}$$

That is, the variation in $\lambda(\alpha;\theta)$ can be computed in terms of a scaled value of $\lambda(\alpha+\frac{\pi}{2};\theta)$ of the flow field sampled at a phase offset of $\pi/2$ rads. This is the key observation that makes it possible to implement an explicit control to achieve wall tracking based on the λ flow vector field. This observation leads to the first result of the paper.

Theorem 1. *Consider a unicycle vehicle with model*

$$\dot{\xi} = (v\cos\theta, v\sin\theta) \tag{5}$$

$$\dot{\theta} = q \tag{6}$$

moving in an environment with a single infinite planar wall. Choose $\theta_r \in [-\pi, \pi]$ to be the constant desired orientation with respect to the wall. Assume the robot moves with speed $v = const.$ and set

$$q := -\int_0^{2\pi} (\lambda(\alpha;\theta) - \lambda(\alpha;\theta_r))\,\lambda(\alpha+\frac{\pi}{2};\theta)\tan\alpha\,\mathrm{d}\alpha. \tag{7}$$

Then $\theta = \theta_r$ is locally exponentially stable.

Proof. Let $x = \theta - \theta_r$ be the local error around the set point and consider a candidate Lyapunov function $E(x)$

$$E(\theta) := \frac{1}{2}\int_0^{2\pi} (\lambda(\alpha;\theta) - \lambda(\alpha;\theta_r))^2\ \mathrm{d}\alpha \tag{8}$$

Since λ is independent of the unknown speed μ then E is a function only of the unknown state θ with parameter θ_r.

Substituting for 3 (using the assumption of a single planar wall), one obtains

$$\begin{aligned}E(\theta) &= \int_0^{2\pi} \sin^2\alpha\,(\sin(\alpha+\theta) - \sin(\alpha+\theta_r))^2\ \mathrm{d}\alpha\\ &= \int_0^{2\pi} x^2\sin^2\alpha\left(1 + \sum_{n=1}^{\infty}\sum_{i=0}^{n}(\alpha+\theta)^i(\alpha+\theta_r)^{n-i}\right)^2\ \mathrm{d}\alpha\\ &= x^2 + O(|x|^3)\end{aligned}$$

where $O(|x|^3)$ denotes higher order terms. It follows that there is a neighbourhood of $x = 0$, and constants $a, b > 0$ such that

$$ax^2 \le E(\theta) \le bx^2.$$

Differentiating E along trajectories of the closed-loop system one obtains

$$\begin{aligned}\frac{dE}{dt} &= \frac{\partial E}{\partial\theta}\frac{\partial\theta}{\partial t}\\ &= \dot{\theta}\int_0^{2\pi} (\lambda(\alpha;\theta) - \lambda(\alpha;\theta_r))\,\frac{\partial\lambda(\alpha;\theta)}{\partial\theta}\,\mathrm{d}\alpha\\ &= q\int_0^{2\pi} (\lambda(\alpha;\theta) - \lambda(\alpha;\theta_r))\,\lambda(\alpha+\frac{\pi}{2};\theta)\tan\alpha\,\mathrm{d}\alpha\\ &= -q^2\end{aligned}$$

Note that $q = x + O(|x|^2)$. That is, there exists a neighbourhood of $x = 0$ such that

$$q^2 \ge ax^2 + \text{higher order terms.}$$

The result follows from standard Lyapunov theory [Khalil, 2001, Th 4.10]. □

Global exponential (or even asymptotic stability) of the heading angle is impossible due to the topological constraints of stabilising a variable on the circle [Bhat and Bernstein, 2000]. Any continuous feedback $q(\theta)$ that has a zero crossing at $\theta = \theta_r$ with negative slope (a requirement for local exponential stability) must also have a zero crossing with positive slope (an unstable equilibria of the closed loop system) somewhere on the circle. In practice, the plot of q can be complex to understand, and for ranges of certain angles, specifically those where the robot is nearly directly approaching or retreating from the wall, there are even stable equilibria that are not the desired stability point. In two specific cases of interest we obtain more definite results:

Set $\theta_r = 0$ to specify a goal of tracking parallel to a wall. Then setting $q = 0$ and solving (7) one finds

$$0 = (2\cos\theta - 3)\sin\theta$$

That is the equilibrium points are $\theta = 0$ (a stable equilibria) and $\theta = \pi$ (an unstable equilibria). In this case there

is an almost globally asymptotic point corresponding to the desired wall tracking behaviour, and a corresponding unstable equilibria, corresponding to the vehicle attempting to move in the wrong direction, but parallel to the wall. A simple perturbation analysis of the system shows that an analogous results holds for all θ_r in a local neighbourhood of $\theta_r = 0$.

To see an example of the difficulties that can occur we consider the case where $\theta_r = \frac{3\pi}{2}$, a situation where the vehicle aims to move directly away from the wall. Setting $q = 0$ and solving (7) one obtains

$$0 = (2\sin\theta - 1)\cos\theta$$

This equation has solutions $\theta = \frac{\pi}{2}, \frac{3\pi}{2}, \frac{\pi}{6}, \frac{5\pi}{6}$. By inspecting the plot of $q(\theta)$ (Figure 2) it is easily verified that $\frac{3\pi}{2}$ and $\frac{\pi}{2}$ are stable equilibria while $\frac{\pi}{6}$ and $\frac{5\pi}{6}$ are unstable equilibria. The basin of attraction of the desired angle $\theta = \theta_r$ is $\theta \in (\frac{5\pi}{6}, \frac{13\pi}{6})$.

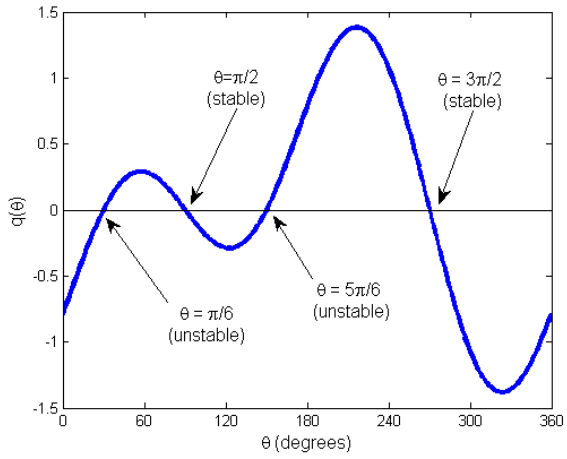

Figure 2: $q(\theta)$ for $\theta_r = 3\pi/2$

One aspect of the proposed control is that it respects the orientation of the desired motion. That is choosing $\theta_r = 0$ will specify that the robot tracks with the wall on its left with respect to its motion, while choosing $\theta_r = \pi$ will track with the wall on the right.

3 Robustness to missing optic flow

A key advantage of the proposed algorithm over many of the earlier approaches in the literature [Serres *et al.*, 2006; Coombs *et al.*, 1995; Herisse *et al.*, 2010; McCarthy *et al.*, 2008; Muratet *et al.*, 2004; Ruffier and Franceschini, 2005; Ruffier *et al.*, 2003; Zufferey and Floreano, 2005; 2006] is that it utilises wide-field optic flow, potentially increasing reliability when there are areas in the image that do not generate optic flow. This section analyses robustness of the proposed algorithm in situations where dense optic flow is not available.

We consider the case where reliable optic flow values are only available over an arbitrary partition of portions of the circle. In order to apply the proposed control construction we will need in addition that any part of the flow field that we use in the control design has a corresponding component of non-null flow offset by $\pi/2$ radians. We make a new partition of the circle into portions of flow by deleting from the initial partition all components of flow that do not have corresponding flow at $\pi/2$ radians offset (the sections of flow shown in red in Fig. 3). Following this process, and due to the natural antipodal symmetry of the flow field λ, the resulting partition has a $\pi/2$ rotational symmetry around the circle (see Fig. 3). That is, the partition can be fully characterized by labelling only the partitions in the first $\pi/2$ radian quadrant of the circle. Let n denote the number of partitions of flow in the first quadrant of the circle and let S_a^i and S_b^i (for $i \in [0, n]$) denote the angles that define this partition in the body fixed frame (see Fig. 3).

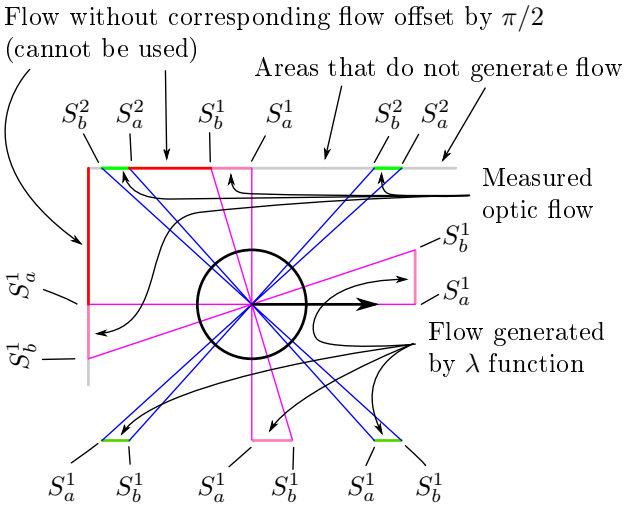

Figure 3: Partial flow scenario

Assume a single planar wall with sparse flow, and include the additional condition that there exists at least one non-null patch of dense flow with a corresponding patch of flow offset by $\pi/2$ radians.

Define an indicator function $\delta(\beta)$ as

$$\delta(\beta) := \begin{cases} 1 & \text{when flow is present at both } \alpha = \beta \\ & \text{and at } \alpha = \beta + \pi/2 \\ 0 & \text{otherwise} \end{cases}$$

We compute $E(\theta)$ as in Equation 8, but including this δ function to remove areas without flow:

$$E(\theta) = \int_0^{2\pi} \delta(\alpha)\left(\lambda(\alpha;\theta) - \lambda(\alpha;\theta_r)\right)^2 \, \mathrm{d}\alpha$$

Re-writing this as a sum of integrals over the n regions S_a^i to S_b^i where $\delta(\alpha) = 1$ we obtain

$$\begin{aligned} E(\theta) &= \sum_{i=0}^{n} \left[\int_{S_a^i}^{S_b^i} \left(\lambda(\alpha;\theta) - \lambda(\alpha;\theta_r)\right)^2 \, \mathrm{d}\alpha \right. \\ &\qquad \left. + \int_{S_a^i}^{S_b^i} \left(\lambda(\alpha+\frac{\pi}{2};\theta) - \lambda(\alpha+\frac{\pi}{2};\theta_r)\right)^2 \, \mathrm{d}\alpha \right] \\ &= \sum_{i=0}^{n} \left[\int_{S_a^i}^{S_b^i} \left(\lambda(\alpha;\theta) - \lambda(\alpha;\theta_r)\right)^2 \right. \\ &\qquad \left. + \left(\lambda(\alpha+\frac{\pi}{2};\theta) - \lambda(\alpha+\frac{\pi}{2};\theta_r)\right)^2 \, \mathrm{d}\alpha \right] \end{aligned}$$

This approach provides a distinction between a lack of optic flow data (eg. against a textureless surface) and zero optic flow (eg. a textured surface that isn't moving). Note that, as found previously, $E = 0$ when $\theta = \theta_r$ and $E \geq 0$ always. We now compute the first and second partial derivatives with respect to θ to show that this is indeed a local minimum.

$$\begin{aligned} \frac{\partial E}{\partial \theta} &= 2 \sum_{i=0}^{n} \int_{S_a^i}^{S_b^i} \left(\lambda(\alpha;\theta) - \lambda(\alpha;\theta_r)\right) \lambda(\alpha+\frac{\pi}{2};\theta) \tan\alpha \\ &\quad - \left(\lambda(\alpha+\frac{\pi}{2};\theta) - \lambda(\alpha+\frac{\pi}{2};\theta_r)\right) \lambda(\alpha;\theta) \cot\alpha \, \mathrm{d}\alpha \end{aligned}$$

It is easy to verify that $\theta = \theta_r$ is a stationary point. Evaluating $\frac{\partial^2 E}{\partial \theta^2}$ at $\theta = \theta_r$ yields

$$\left.\frac{\partial^2 E}{\partial \theta^2}\right|_{\theta=\theta_r} = \int_{S_0}^{S_1} 2\sin^2(2\alpha + \theta_r) + 2\sin^2\theta_r \, \mathrm{d}\gamma > 0.$$

Using a similar argument to Theorem 1 it is straightforward to show that $\theta = \theta_r$ is locally asymptotically stable for the control $q = -\frac{\partial E}{\partial \theta}$.

3.1 Simulations of partial flow scenario

MATLAB simulations were used to test the effect of having only partial optic flow available (Figure 4). The negative slope of the intersection point at 0° indicates that both scenarios are locally exponentially stable, and indeed, it is easily seen that both scenarios are in fact almost globally stable, with the unstable point at 180°. The exponent of stability (that is the coefficient in the exponential bound on the convergence of solutions around 0°) is proportional to the slope of the curve at the intersection point 0° in Figure 4. With full flow measurements it is clear that one obtains a significantly larger exponent of stability and the resulting control will provide more robust tracking.

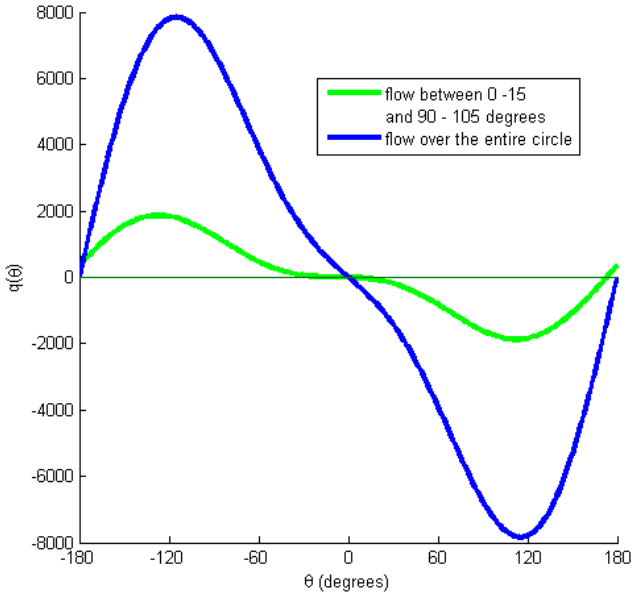

Figure 4: $q(\theta)$ for $\theta_r = 0$ degrees (ie wall following) with varying amounts of flow present

4 Simulation results for non-holonomic vehicle moving in the plane

A small Java simulation was written to perform simulations for a unicycle model of the non-holonomic vehicle in closed loop with the proposed command (7). In the simulation, we are interested how the vehicle moves in a complex environment that does not satisfy the single planar wall assumptions under which the control was derived. We do make the assumption that the sensing system measures dense optic flow. This is approximated by simulating a value of the translational optic flow at eighty points equally spaced around the circumference of the circle.

The pure wall tracking problem, where the particular direction the wall is to be tracked is not specified, is considered in the first simulation. In this case, two λ functions are generated, one at $\theta_r = 0$ and one at $\theta_r = \pi$. Each is compared to the measured flow, and the one with the smaller total error is chosen. In the case where the error is equal, then $\theta_r = 0$ is chosen. This switching control eliminates the presence of the unstable equilibrium in the system response, and replaces it with two stable equilibria, each of which is attractive on half the unit circle of angles. It is not expected that this discontinuity will be seen in practice.

One limitation of the proposed approach is that it does not explicitly stabilise distance from the wall. Hence the vehicle can drift in or out from the wall. This is visible at point (I) in Figure 5. A second effect is that when the assumption of a planar wall fails to hold and specifi-

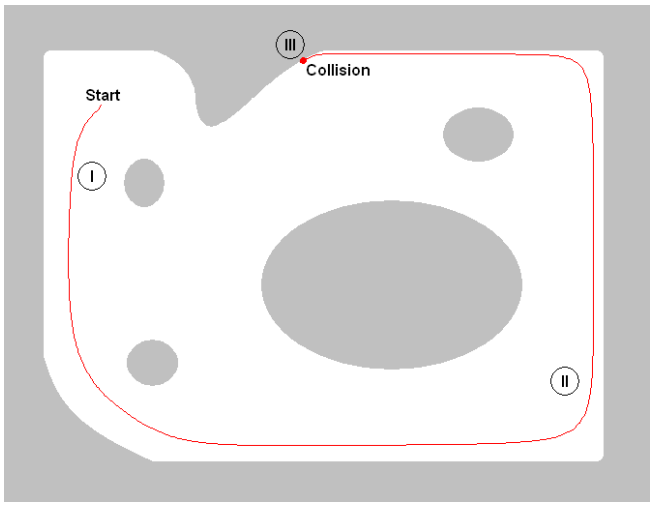

Figure 5: 2D wall following simulation

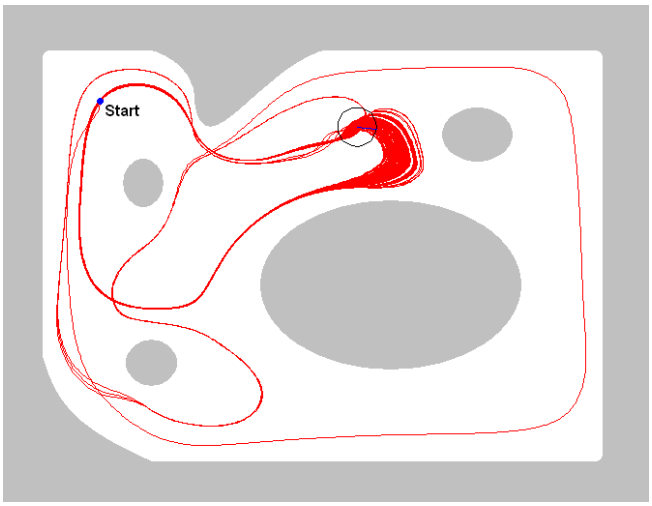

Figure 6: 2D wall following simulation with additional control (one hour simulation)

cally when moving at corners the vehicle can significantly change its distance to the wall (II). Indeed, given that the simulation runs in discrete time and that the flow is noisy due to quantisation error in the depth computation, this can cause the robot to collide with the wall as seen at (III).

This limitation can be addressed in an ad-hoc way by introducing a time varying reference θ_r. Let μ_r be a reference value for a desired total flow, chosen based on the desired tracking offset for a nominal value of the vehicle speed v. We then set

$$\theta_r = \arctan\left(k(\mu_r - \mu)\right),$$

for a positive gain $k > 0$ and using μ as calculated in Equation 2. Assuming that the vehicle is moving with constant speed, then this modification will steer the reference direction of the vehicle to ensure that the vehicle tracks the wall with constant distance. This modification of the proposed control overcomes the tendency of the vehicle to drift towards and away from the wall. This is illustrated in Figure 6. In addition to improving the wall tracking performance, this modification also improves the behaviour when the vehicle encounters an acute angle turn. In this case the sudden increase in optic flow magnitude as the vehicle becomes trapped in the corner forces the desired steering angle $\theta_r \to \pi/2$, associated with a pure obstacle avoidance behaviour. As long as the system dynamics are capable of reproducing the specified closed-loop response, the vehicle will not collide in the corner.

To investigate the impact of dense but noisy flow, the simulator was modified to add Gaussian noise with mean 0 and standard deviation 0.003 to the measured optic flow. The average magnitude of the measured optic flow is roughly 0.0258. With these settings the simulator completed a 12-hour run without colliding with any walls, as shown in Figure 7. Note that when the robot moves sufficiently far from a wall, the noise dominates and the robot drives randomly until it approaches another wall.

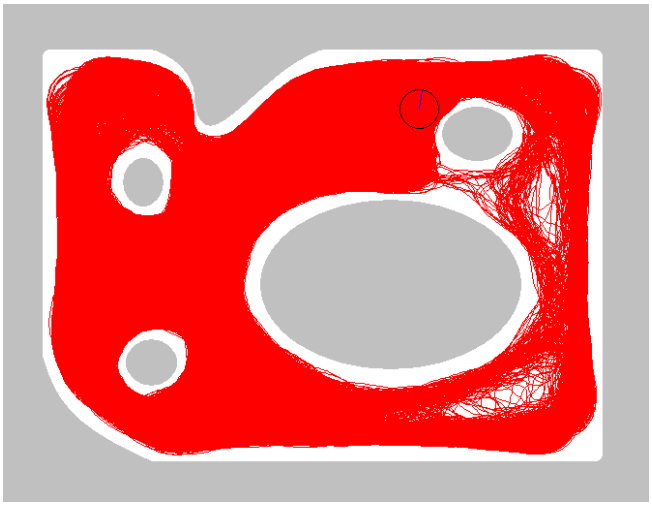

Figure 7: Noisy wall-following simulation with additional control (twelve hour simulation)

5 3D non-holonomic derivation

In this section, the equivalent three dimensional control problem is considered where a non-holonomic vehicle is moving in the presence of an infinite planar surface. An example of a vehicle that moves in 3D with an approximate non-holonomic assumption on its velocity is a fixed-wing drone. For such vehicle the linear velocity of the

vehicle is always in the same direction in the body-fixed frame, up to small variations due to changes in angle of attack and external wind disturbances. It should be noted that this problem is qualitatively more difficult that the two dimensional case since in this case the optic flow is defined on the sphere S^2 that is not an orientable manifold, and hence there is no simple way of defining a direction for the flow.

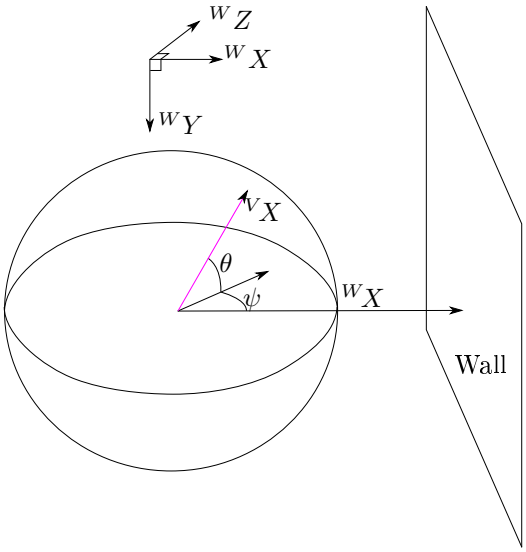

Figure 8: 3D scenario

Without loss of generality the infinite plane is modelled in the world Y-Z axes. The important frames are $\{W\}$ (world frame), $\{B\}$ (body-fixed frame), $\{\Gamma\}$ (integration frame) and $\{V\}$ (velocity frame). We assume that $\{B\} = \{V\}$ by choosing the body-fixed frame to correspond to the non-holonomic constraints on the vehicle velocity. Optic flow is measured on the surface of a sphere in the body-fixed frame, and will be a 3D vector at each point.

Define the wall/terrain to be in the $+^W X$ direction (world frame), the velocity to be in the $+^V X$ direction (velocity frame), and the integration angle to be in the $+^\Gamma X$ direction (integration frame). The rotations between these frames are described by rotation matrices

$$ {}^W_V R = R_y(\psi) R_z(\theta), \qquad {}^\Gamma_V R = R_y(\beta) R_z(\alpha) $$

where $R_y(\psi)$ is the Euler-angle rotation matrix describing a rotation of β around the Y axis. The scenario is illustrated in Figure 8.

Define a vector for the integration direction in the vehicle frame ${}^V\gamma$

$$ {}^V\gamma = {}^\Gamma_V R^T \begin{bmatrix} 1 \\ 0 \\ 0 \end{bmatrix} = \begin{bmatrix} \cos\alpha\cos\beta \\ -\sin\alpha\cos\beta \\ \sin\beta \end{bmatrix} $$

In 3D, the optic flow measured on a sphere is written as two separate parts:

$$ \phi_D(\alpha,\beta;\psi,\theta) = \frac{1}{d}\left({}^W_V R\, {}^V\gamma \cdot \begin{bmatrix} 1 \\ 0 \\ 0 \end{bmatrix} \right) $$

$$ \phi_V(\alpha,\beta;\psi,\theta) = v\left(\left(\begin{bmatrix} 1 \\ 0 \\ 0 \end{bmatrix} \times {}^V\gamma \right) \times {}^V\gamma \right) $$

$$ \phi(\alpha,\beta;\psi,\theta) = \begin{cases} \phi_D\, \phi_V & \text{for the side towards the wall} \\ 0 & \text{otherwise} \end{cases} $$

ϕ_D represents the scalar distance to the wall, measured along the integration direction γ in the body fixed frame. ϕ_V is a vector quantity that computes the portion of velocity perpendicular to the integration direction.

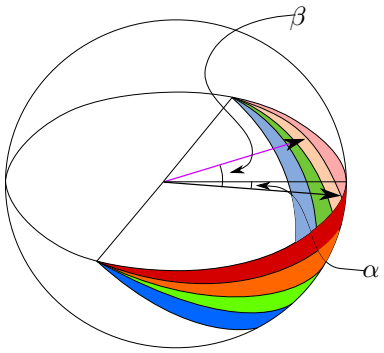

Figure 9: Construction of κ in the 3D case. Integration occurs across the coloured bands

Define a function κ as

$$ \begin{aligned} \kappa &= \int_{-\pi/2}^{\pi/2} \Big(\phi(\alpha,\beta;\psi,\theta) - \phi(\alpha+\pi,\pi-\beta;\psi,\theta) \Big)\, \mathrm{d}\beta \\ &= \frac{2\mu}{3} \begin{bmatrix} \cos\psi\cos(\alpha-\theta)\,(\cos(2\alpha)-2) \\ -2\sin\alpha\cos\alpha\cos\psi\cos(\alpha-\theta) \\ \cos\alpha\sin\psi \end{bmatrix} \end{aligned} $$

The purpose of κ is to integrate across the coloured bands shown in Figure 9, thereby eliminating one dimension from the problem. The Z component is removed without loss of information, as the flow is known to exist on the (2D) surface of the sphere and can therefore be fully defined by only two values.

$$ \begin{aligned} \kappa_{xy} &= \begin{bmatrix} 1 & 0 & 0 \\ 0 & 1 & 0 \\ 0 & 0 & 0 \end{bmatrix} \kappa \\ &= \frac{2\mu}{3} \begin{bmatrix} \cos\psi\cos(\alpha-\theta)\,(\cos(2\alpha)-2) \\ -2\sin\alpha\cos\alpha\cos\psi\cos(\alpha-\theta) \\ 0 \end{bmatrix} \end{aligned} $$

The result is normalised to eliminate the effect of μ:

$$\mu^2 = \frac{4}{\pi^2}\left[\left(\int_0^{2\pi}\cos\alpha\kappa_y\,\mathrm{d}\alpha\right)^2 + \left(\int_0^{2\pi}\sin\alpha\kappa_y\,\mathrm{d}\alpha\right)^2 + \left(\frac{1}{2}\int_0^{2\pi}\cos\alpha\kappa_z\,\mathrm{d}\alpha\right)^2\right]$$

$$\lambda_{xy} = \frac{\kappa_{xy}}{\sqrt{\mu^2}}$$

The quantity $\frac{\partial\lambda_{xy}}{\partial\theta}$ is analogous to the 2D case:

$$\frac{\partial\lambda_{xy}}{\partial\theta} = \begin{bmatrix} \frac{2-\cos(2\alpha)}{2+\cos(2\alpha)} & 0 & 0 \\ 0 & -1 & 0 \\ 0 & 0 & 0 \end{bmatrix} \lambda_{xy}\left(\alpha - \frac{\pi}{2}; \theta, \psi, m\right)$$

Consider a vehicle with model

$$\dot{\xi} = (v\cos\theta\cos\psi, v\sin\theta, -v\cos\theta\sin\psi)$$
$$\dot{\theta} = q$$

where q is defined as

$$q = -\int_0^{2\pi}\left(\lambda_{xy}\left(\alpha;\theta,\psi,m\right) - \lambda_{xy}\left(\alpha;\theta_r,\psi_r\right)\right) \cdot \frac{\partial\lambda_{xy}\left(\alpha;\theta,\psi\right)}{\partial\theta}\,\mathrm{d}\alpha.$$

We claim that, using this q, E will decrease over time to reach a minimum and this minimum will correspond to correct wall-following behaviour. To support this claim, consider the analogue cost function to Equation 8:

$$E(\theta,\psi) = \frac{1}{2}\int_0^{2\pi}\left(\lambda_{xy}\left(\alpha;\theta,\psi\right) - \lambda_{xy}\left(\alpha;\theta_r,\psi_r\right)\right)^2\,\mathrm{d}\gamma$$

We calculate the derivative of E with respect to time when using the given control law, to show that it will decrease or at least remain constant.

$$\begin{aligned}\frac{\mathrm{d}E(\theta,\psi)}{\mathrm{d}t} &= \frac{\partial E}{\partial\theta}\frac{\partial\theta}{\partial t} \\ &= \dot{\theta}\int_0^{2\pi}\left(\lambda_{xy}\left(\alpha;\theta,\psi\right) - \lambda_{xy}\left(\alpha;\theta_r,\psi_r\right)\right) \cdot \frac{\mathrm{d}\lambda_{xy}\left(\alpha;\theta,\psi\right)}{\mathrm{d}\theta}\,\mathrm{d}\alpha \\ &= -q^2\end{aligned}$$

As $E(\theta,\psi)$ will not increase and that $E(\theta_r,\psi_r) = 0$, we claim that the vehicle will experience local stability around $\theta = \theta_r, \psi = \psi_r$.

6 Conclusion and future directions

This approach shows promise for wall following and collision avoidance in 2D and 3D vehicles. Use of wide-field flow offers excellent stability, particularly when following walls where the vehicle will eventually converge to the correct direction from almost any initial conditions. However, much work remains to be done. Stability must be proven in the 3D case, and both 2D and 3D algorithms must be tested in real-world scenarios.

Use of a holonomic vehicle (eg. most rotorcraft) rather than a fixed-wing UAV will require that the algorithm is extended to cover scenarios where the velocity direction may vary in the body-fixed frame. This extension would also make the 2D case suitable for use on a hovercraft.

To perform useful work, this system needs to be combined with higher-level control strategies that suggest a general direction to move in. A simple additive system may work well here; when near a wall the extremely high control values from the wall following algorithm will dominate, and when the robot is distant from walls or centred in a corridor the wall following control input goes to zero and allows the higher-level control to take over.

References

[Andreasson *et al.*, 2007] Henrik Andreasson, Tom Duckett, and Achim Lilienthal. Mini-slam: Minimalistic visual slam in large-scale environments based on a new interpretation of image similarity. In *In Proc. of the 2007 IEEE International Conference on Robotics and Automation (ICRA)*, pages 4096–4101, 2007.

[Bhat and Bernstein, 2000] Bhat and Bernstein. A topological obstruction to continuous global stabilization of rotational motion and the unwinding phenomenon. *Systems & Control Letters*, 39(1):63 – 70, 2000.

[Bryson and Sukkarieh, 2007] M. Bryson and S. Sukkarieh. Building a robust implementation of bearing-only inertial slam for a uav. *Journal of Field Robotics*, 24(1-2):113 – 143, 2007.

[Coombs *et al.*, 1995] D. Coombs, M. Herman, Tsai Hong, and M. Nashman. Real-time obstacle avoidance using central flow divergence and peripheral flow. In *ICCV '95: Proceedings of the Fifth International Conference on Computer Vision*, page 276, Washington, DC, USA, 1995. IEEE Computer Society.

[Davison *et al.*, 2007] Andrew J. Davison, Ian D. Reid, Nicholas D. Molton, and Olivier Stasse. Monoslam: Real-time single camera slam. *IEEE Transactions on Pattern Analysis and Machine Intelligence*, 29:1052–1067, 2007.

[Herisse *et al.*, 2010] B. Herisse, S. Oustrieres, T. Hamel, R. Mahony, and F.-X. Russotto. A general optical flow based terrain-following strategy for a vtol uav using multiple views. In *Robotics and Automation (ICRA), 2010 IEEE International Conference on*, pages 3341 –3348, May 2010.

[Humbert *et al.*, 2009] J. Sean Humbert, Joseph K. Conroy, Craig W. Neely, and Geoffrey Barrows. Wide-field integration methods for visuomotor control. In Dario Floreano, Jean-Christophe Zufferey, Mandyam V. Srinivasan, and Charlie Ellington, editors, *Flying Insects and Robots*, pages 63–71. Springer Berlin Heidelberg, 2009.

[Khalil, 2001] H. Khalil. *Nonlinear Systems*. Prentice-Hall, 3 edition, December 2001.

[Kim and Sukkarieh, 2007] Jonghyuk Kim and Salah Sukkarieh. Real-time implementation of airborne inertial-slam. *Robotics and Autonomous Systems*, 55(1):62 – 71, 2007. Simultaneous Localisation and Map Building.

[Lim and Barnes, 2010] John Lim and Nick Barnes. Estimation of the epipole using optical flow at antipodal points. *Computer Vision and Image Understanding*, 114(2):245 – 253, 2010. Special issue on Omnidirectional Vision, Camera Networks and Non-conventional Cameras.

[McCarthy *et al.*, 2008] C. McCarthy, N. Barnes, and R. Mahony. A robust docking strategy for a mobile robot using flow field divergence. *IEEE Transactions on Robotics*, 24(4), 2008.

[Muratet *et al.*, 2004] Muratet, Doncieux, and Meyer. A biomimetic reactive navigation system using the optic flow for a rotary-wing uav in urban environment. In *Proceedings of the International Session on Robotics*, 2004.

[Ruffier and Franceschini, 2005] Franck Ruffier and Nicolas Franceschini. Optic flow regulation: the key to aircraft automatic guidance. *Robotics and Autonomous Systems*, 50(4):177 – 194, 2005. Biomimetic Robotics.

[Ruffier *et al.*, 2003] F. Ruffier, S. Viollet, S. Amic, and N. Franceschini. Bio-inspired optical flow circuits for the visual guidance of micro-air vehicles. In *Proceedings of the IEEE International Symposium on Circuits and Systems*, volume III, pages 846 – 849. IEEE Computer Society, 2003.

[Santos-Victor *et al.*, 1995] Santos-Victor, Sandini, Curotto, and Garibaldi. Divergent stereo in autonomous navigation: From bees to robots. *International Journal of Computer Vision*, 14:159 – 177, 1995.

[Serres *et al.*, 2006] Serres, Ruffier, Viollet, and Franceschini. Toward optic flow regulation for wall-following and centring behaviours. *International Journal of Advanced Robotic Systems*, 3(2):147 – 154, 2006.

[Srinivasan *et al.*, 1996] M Srinivasan, S Zhang, M Lehrer, and T Collett. Honeybee navigation en route to the goal: visual flight control and odometry. *J Exp Biol*, 199(1):237–244, 1996.

[Srinivasan *et al.*, 1999a] M. V. Srinivasan, J. S. Chahl, K. Weber, S. Venkatesh, M. G. Nagle, and S. W. Zhang. Robot navigation inspired by principles of insect vision. *Robotics and Autonomous Systems*, 26(2-3):203 – 216, 1999. Field and Service Robotics.

[Srinivasan *et al.*, 1999b] Mandyam V. Srinivasan, Michael Poteser, and Karl Kral. Motion detection in insect orientation and navigation. *Vision Research*, 39(16):2749 – 2766, 1999.

[Vassallo *et al.*, 1998] Vassallo, Schneebeli, and Santos-Victor. Visual navigation: Combining visual servoding and appearance based methods. In *6th International Symposium on Intelligent Robotic Systems*, July 1998.

[Zufferey and Floreano, 2005] Jean-Christophe Zufferey and Dario Floreano. Toward 30-gram autonomous indoor aircraft: Vision-based obstacle avoidance and altitude control. 2005.

[Zufferey and Floreano, 2006] Jean-Christophe Zufferey and Dario Floreano. Fly-inspired visual steering of an ultralight indoor aircraft. 2006.